Theoretical approach to explore the production routes of astatine radionuclides

Moumita Maiti and Susanta Lahiri
Chemical Sciences Division, Saha Institute of Nuclear Physics, 1/AF, Bidhannagar, Kolkata 700 064, India
(Received 15 December 2008; published 19 February 2009)

To fulfill the recent thrust of astatine radionuclides in the field of nuclear medicine, various production routes have been explored in the present work. The possible production routes of $^{209-211}$At comprise both light- and heavy-ion-induced reactions at the bombarding energy range starting from threshold to a maximum of 100 MeV. Excitation functions of those radionuclides, produced through various production routes, have been calculated by using nuclear reaction model codes TALYS, ALICE91, and PACE-II and are compared with the available measured data. Contributions of various reaction mechanisms, such as direct, pre-equilibrium, and equilibrium reactions, to the total reaction cross section have been studied using the codes. Results show that the equilibrium reaction dominates in all cases over other reaction mechanisms.

DOI: 10.1103/PhysRevC.79.024611 PACS number(s): 24.10.−i, 25.55.−e, 25.70.−z, 27.90.+b

I. INTRODUCTION

In the past decade radionuclides of the semimetallic element astatine (At) has drawn ample attention in the field of nuclear medicine. Nuclear physics has an important role in developing this field as producing At radionuclides through nuclear reactions is the method of choice. Most of the identified radioisotopes of At are short-lived. ^{210}At, with $T_{1/2} = 8.1$ h, is the most stable isotope. Astatine radioisotopes are produced artificially, however, in the Earth's crust, where a small amount of At may last in equilibrium with uranium and thorium. Astatine was discovered about 80 years ago but studies on its chemical properties faced practical constraints owing to its scarcity and short half-life. Recent reports on chemical separation of At radionuclides from the bulk, an important step before its *in vivo* application, have been cited in Refs. [1–3]. A list of At radionuclides with suitable half-lives that may find possible use in nuclear medicine is presented in Table I.

Among others, ^{211}At is the most promising radionuclide for targeted therapy owing to its suitable half-life and relatively high linear energy transfer (LET) of α particles in human tissues. ^{211}At has two major decay modes, both of which eventually emit high-energy α particles suitable for targeted therapy. The α-decay mode emits an α particle with an energy of 5.867 MeV, leaving ^{207}Bi ($T_{1/2} = 32.9$ yr) as a residual, which decays to stable ^{207}Pb. Other decay modes produce an ultra-short-lived daughter, ^{211g}Po ($T_{1/2} = 516$ ms, $J = 9/2^+$), which decays to stable ^{207}Pb by emitting a 7.45-MeV α particle along with the emission of X rays. The metastable state of ^{211m}Po ($T_{1/2} = 25.2$ s, $J = 25/2^+$) is not populated by ^{211}At because of its high spin and low transition probabilities. The γ-emitting radionuclides ^{209,210}At have mostly ϵ-capture decay mode and produce the long-lived α-emitting ^{209,210}Po daughters. These At radionuclides may also find uses in diagnosis because of their suitable half-life and high-intensity γ rays.

Radionuclidic purity is an important issue in nuclear medicine. Therefore, At radionuclide for medical application has to be obtained in its purest form to avoid additional radiation exposure from impurities. In general, the production route and the chemical separation technique are the two major sources of impurities (radionuclides as well as stable). The production route hosts radionuclidic impurities and their corresponding decay products including the decay of the compound nucleus. Optimization of nuclear reaction parameters, such as suitable target-projectile combination, bombarding energy of projectile, thickness of target, etc., can reduce the production of certain impurities. For example, the most commonly used production route of At radionuclides is ^{209}Bi$(\alpha, xn)^{209-211}$At [5–11]. These At isotopes and their daughter products (radioactive and stable) can be considered as impurities when a particular isotope is desired. Long-lived impurities are hazardous to human health if the injected amount goes above a certain level, and the stable heavy metals, Pb and Tl (the end products of At radioisotopes), are sometimes carcinogenic and affect human metabolism. The judicious choice of the bombarding energy of the α particle helps to reduce radionuclidic impurities.

Astatine radionuclides can be produced either directly by choosing suitable target-projectile combinations or from the decay of its precursor Rn isotopes. Direct production of $^{209-211}$At is possible by light- and heavy-ion-induced reactions in low- and medium-energy accelerators. High-energy-proton-induced spallation reactions on heavy targets such as ^{238}U and ^{232}Th can also be used to produce $^{209-211}$At. In the indirect method, $^{209-211}$Rn ($T_{1/2} = 28.5$ m, 2.4 h, and 14.6 h, respectively) isotopes are produced in a similar fashion either by light-charged-particle-induced reactions or by spallation reactions induced by high-energy protons and $^{209-211}$At isotopes are obtained as a daughter product of $^{209-211}$Rn. Various production routes of $^{209-211}$At escort different types of impurities whose quantification is important for their application in nuclear medicine.

The present work is to explore the possible production routes of $^{209-211}$At radionuclides from both light- and heavy-ion-induced reactions. Production of At radionuclides is preferred from the α-induced reaction on ^{209}Bi because of the high yield required for therapeutic purposes. However, productions via light- and heavy-ion-induced reactions may serve other scientific purposes (e.g., biological studies requiring a minute amount of radioactivity). We aim in this paper to investigate theoretically the various possible production routes of $^{209-211}$At from both light- and heavy-ion-induced

TABLE I. The nuclear properties [4] of At radionuclides useful in the field of nuclear medicine.

Radionuclide	$T_{1/2}$ (h)	Decay mode	α (MeV)	γ (keV)(%)
^{211}At	7.214	ϵ 58.2%, α 41.8%	5.867	687(0.246)
^{210}At	8.1	ϵ 99.82%, α 0.18%	5.524, 5.361	1181.43(99.3), 245.35(79), 1483.35(46.5)
^{209}At	5.41	ϵ 95.9%, α 4.1%	5.647	545.03(91), 781.89(83.5), 790.2(63.5)
^{208}At	1.63	ϵ 99.45%, α 0.55%	5.641	685.2(97.89), 660.1(90), 177.0(46)

reactions and the reaction mechanisms involved in each route. A comparison of theoretically predicted production cross sections has been made with the reported experimental values wherever available.

Production of $^{209-211}$At radionuclides from light- (α and ^{3}He) and heavy-ion- (^{6,7}Li, ^{9}Be) induced reactions on heavy natural targets such as Bi, Pb, and Tl involves mostly pre-equilibrium (PEQ) and equilibrium (EQ) reaction mechanisms in the low- and medium-energy range. For high projectile energy, the direct reaction (DIR) mechanism may also have some contribution. A composite nucleus is formed when a target is bombarded by the projectile of a certain energy. Particle emission may occur from any stage of the relaxation process of the target-projectile composite system, leaving the residual in an excited state. The excited residual nucleus is cooled either by particle emission (if the residual excitation is higher than the particle emission threshold giving birth to a new residual nucleus) or by γ-ray emission.

For the direct reaction, particles are emitted because of the large momentum transfer from the very first interaction between the projectile and the target. As a result, the ejectile carries high energy, leaving the residual at lower excitation. When the incoming energy of the projectile is shared by all the nucleons of the composite system, an equilibrium condition is reached. Particles are emitted from the compound nucleus because of statistical fluctuations in energy. Therefore, compound nuclear emissions are low-energy emissions and the residual is left at high excitation energy.

Between the two extremes, there is an intermediate stage of reaction that exhibits both direct and compound-like features. These reactions are referred to as PEQ processes. PEQ emissions take place after the first stage of the reaction (DIR) but long before statistical equilibrium of the compound nucleus is attained. PEQ processes cover a significant part of the reaction cross section for incident energies between 10 and 200 MeV. The production cross section of the desired radionuclide is the resultant of all the reaction mechanisms involved.

Light- and heavy-ion-induced nuclear reactions have been studied by using the nuclear reaction model codes TALYS [12], ALICE91 [13,14], and PACE-II [15]. The code TALYS takes into account all three types of reaction mechanisms: DIR [coupled channel analysis, distorted-wave Born approximation (DWBA), etc.], PEQ (one- and two-component exciton models), and EQ (Hauser-Feshbach model). PACE-II accounts only for evaporation reactions based on the Hauser-Feshbach model [16], and ALICE91 considers PEQ (hybrid model) along with the EQ reactions (Weisskopf-Ewing model) [17]. A list of reactions studied in the present work is presented in Table II. Use of these codes enables us to understand the reliability as well as predictability of the codes.

In the next section we give a brief description of the codes TALYS, ALICE91, and PACE-II and the input option used for the present calculation. Section III shows the remarkable features of the codes. In Sec. IV we discuss the results obtained in the present study.

II. BRIEF DESCRIPTION OF NUCLEAR REACTION MODEL CODES

A. ALICE91

We have used the code ALICE91 [13,14] to calculate the excitation function of At radionuclides produced through various reaction mechanisms. A geometry-dependent hybrid model [14,18–20] has been used to calculate PEQ emissions and the Weisskopf-Ewing formalism [17] for EQ emissions. ALICE91 does not consider DIR emissions. The hybrid model is a combination of an exciton model [21] and the Boltzmann master equation approach [22,23]. It assumes that the target-projectile composite system proceeds through two-body interaction process. Each stage of the relaxation

TABLE II. List of nuclear reactions studied along with corresponding Q values and threshold energies.

Reaction	Q value (MeV)	E_{th}(MeV)
^{209}Bi(α, $2n$)^{211}At	−20.33	20.72
^{209}Bi(α, $3n$)^{210}At	−28.07	28.61
^{209}Bi(α, $4n$)^{209}At	−35.24	35.92
^{209}Bi(^{3}He, n)^{211}At	0.25	0
^{209}Bi(^{3}He, $2n$)^{210}At	−7.50	7.61
^{209}Bi(^{3}He, $3n$)^{210}At	−14.66	14.87
^{208}Pb(^{6}Li, $3n$)^{211}At	−20.23	20.81
^{208}Pb(^{6}Li, $4n$)^{210}At	−27.98	28.78
^{208}Pb(^{6}Li, $5n$)^{209}At	−35.14	36.15
^{208}Pb(^{7}Li, $4n$)^{211}At	−27.48	28.41
^{208}Pb(^{7}Li, $5n$)^{210}At	−35.23	36.41
^{208}Pb(^{7}Li, $6n$)^{209}At	−42.39	43.82
^{203}Tl(^{9}Be, n)^{211}At	−10.84	11.32
^{203}Tl(^{9}Be, $2n$)^{210}At	−18.58	19.41
^{203}Tl(^{9}Be, $3n$)^{210}At	−25.75	26.89
^{205}Tl(^{9}Be, $3n$)^{211}At	−25.04	26.14
^{205}Tl(^{9}Be, $4n$)^{210}At	−32.79	34.23
^{205}Tl(^{9}Be, $5n$)^{209}At	−39.95	41.71

process is designated by the total number (n) of excited particles, that is, the sum of the excited particles (p) and holes (h). In each two-body interaction, a p-h pair may be created or annihilated or redistribution of energy takes place without changing the number. The hybrid model uses a "never come back" approximation; that is, the model assumes that only one p-h pair is created in each interaction. The hybrid model explicitly determines the pre-emission energy distribution of the excited particles, which helps to estimate high-energy emissions more accurately. The geometry-dependent hybrid model includes nuclear surface effects [14,19,20]. The PEQ emission cross section for a particular ejectile x with energy ϵ_x is given by

$$\sigma_{\mathrm{PEQ}}(\epsilon_x) = \frac{\lambda^2}{4\pi}\sum_{l=0}^{\infty}(2l+1)T_l \sum_{\substack{n=n_0,\\ \Delta n=2}}^{\overline{n}} D_n \left[f_n^x \frac{N_n(l,U,\epsilon_x)}{N_n(l,E_c)}\right] \times \frac{\lambda_c(\epsilon_x)}{\lambda_c(\epsilon_x)+\lambda_t(\epsilon_x)}, \quad (1)$$

where λ is the de Broglie wavelength of the projectile, T_l is the transmission coefficient of the lth partial wave, D_n is the depletion factor of the nth exciton state, that is, probability of reaching n exciton state without prior emission, and f_n^x is the number of x type excited nucleons present in it. The numbers n_0 and $\overline{n}$ are the initial and equilibrium exciton numbers, respectively. The ratio $N_n(l,U,\epsilon_x)/N_n(l,E_c)$ is the probability of finding x type nucleons in the n exciton state with energy $\epsilon_x + B_x$, where B_x is the separation energy of x. The factor $\frac{\lambda_c(\epsilon_x)}{\lambda_c(\epsilon_x)+\lambda_t(\epsilon_x)}$ is the emission probability of x with energy ϵ_x. $\lambda_t(\epsilon_x)$ is the two-body interaction rate. The emission rate $\lambda_c(\epsilon_x)$ is calculated by [14]

$$\lambda_c(\epsilon_x) = \frac{(2S_x+1)\mu_x\epsilon_x\sigma_{\mathrm{inv}}(\epsilon_x)}{\pi^2\hbar^3 g}, \quad (2)$$

where S_x is the intrinsic spin of x, μ_x is the reduced mass, σ_{inv} is the inverse cross section of the ejectile x with energy ϵ_x being absorbed by the residual, and g is the single-particle level density of the composite nucleus. The EQ emission cross section is calculated by using the Weisskopf-Ewing formalism as

$$\sigma_{\mathrm{EQ}}(\epsilon_x) \sim \sigma_{\mathrm{comp}} \frac{e^{2(aU)^{1/2}}}{U}, \quad (3)$$

where σ_{comp} is the compound nuclear formation cross section, a is the level density parameter, and U is the available excitation energy of the compound nucleus after the PEQ emissions. The cross section σ_{comp} is calculated as $\sigma_{\mathrm{comp}} = \sigma_{\mathrm{abs}} - \sigma_{\mathrm{PEQ}}$, where σ_{abs} is the absorption cross section of the projectile in the target and σ_{PEQ} is the total PEQ emission cross section.

The calculations have been performed using the code ALICE91 [13,14] with a geometry-dependent hybrid model for PEQ emissions and the Weisskopf-Ewing formalism for EQ emissions. Neutron, proton, α, and deuteron emissions are considered from the residual nuclides of 12 mass units wide and 10 charge units deep including the composite nucleus. The Fermi gas level density has been used for the calculation of reaction cross sections. Reverse channel reaction cross sections have been calculated using the optical model. A default value of the level density parameter of $A/9$ has been chosen for the calculation. The total number of nucleons in the projectile has been chosen as the initial exciton number for the cross-section calculation.

B. TALYS

The code TALYS [12] has been used to calculate the production of At radionuclides through α-particle- and ^{3}He-induced reactions on a ^{209}Bi target. We have adopted a two-component exciton model for the estimation of PEQ emissions, a detailed Hauser-Feshbach formalism [16] for the EQ emissions, and a coupled channel analysis for the DIR reaction process. For PEQ reactions involving projectiles and ejectiles heavier than nucleon (d, t, ^{3}He, and α particles) direct-like reaction processes, stripping, pickup, and knockout reactions make important contributions in addition to the exciton model and these are treated in the framework of Kalbach's phenomenological model [24] as these processes are not included in the exciton model.

In the two-component exciton model, the total exciton number is divided into proton (p_p) and neutron (p_n) particle number and proton (h_p) and neutron (h_n) hole number. $n_p(=\mathrm{p}_p+\mathrm{h}_p)$ and $n_n(=\mathrm{p}_n+\mathrm{h}_n)$ are the proton and neutron exciton numbers, respectively. The PEQ cross section of the particle x with energy ϵ_x is calculated as

$$\sigma_{\mathrm{PEQ}}(\epsilon_x) = \sigma^{\mathrm{CF}} \sum_{p_p=p_p^0}^{\overline{p}_p}\sum_{p_n=p_n^0}^{\overline{p}_n} D(\mathrm{p}_p,\mathrm{h}_p,\mathrm{p}_n,\mathrm{h}_n) \times W(\mathrm{p}_p,\mathrm{h}_p,\mathrm{p}_n,\mathrm{h}_n,\epsilon_x)\tau(\mathrm{p}_p,\mathrm{h}_p,\mathrm{p}_n,\mathrm{h}_n), \quad (4)$$

where σ^{CF} is the composite nucleus formation cross section, $D(\mathrm{p}_p,\mathrm{h}_p,\mathrm{p}_n,\mathrm{h}_n)$ is the fraction of the PEQ population that has survived previous emission, $W(\mathrm{p}_p,\mathrm{h}_p,\mathrm{p}_n,\mathrm{h}_n,\epsilon_x)$ is the emission rate of x with energy ϵ_x, and τ is the mean lifetime of that state. Compound nuclear emission is calculated in TALYS by two different mechanisms: the binary compound cross section, which is the capture of the projectile in the target nucleus and subsequent emission of a particle or γ ray at low energy, and multiple compound emissions, that is, multiple emissions of the highly excited residual nuclei formed after the binary reaction. Width fluctuation is taken into account in the binary compound cross section. Multiple compound and precompound emissions are considered in the framework of the Hauser-Feshbach and exciton model. TALYS contains both macroscopic and microscopic level densities. The macroscopic level densities are

(i) a constant-temperature model [25] and the Fermi gas model,
(ii) the back-shifted Fermi gas model, and
(iii) a generalized superfluid model.

The code TALYS uses a detailed Hauser-Feshbach formalism for multiple particle emission in the evaporation calculation along with width fluctuation corrections using the Moldauer model [26,27]. The option for multiple PEQ emissions has been chosen within the framework of two-component exciton

model calculation with surface correction to account for the PEQ emissions. We have calculated level densities using a combination of the constant-temperature model by Gilbert and Cameron [25] and the Fermi gas model. The total excitation energy range is divided into two regions: a low-energy part and a high-energy part. The low-energy part starts from 0 MeV to a certain energy, E_{mid}, up to which the constant-temperature law is valid. The high-energy part starts above E_{mid} and the Fermi gas model is used to calculate level densities in this zone.

C. PACE-II

The code PACE-II is the modified version of the Monte Carlo code Projection Angular-momentum Coupling Evaporation. The de-excitation process of the excited nuclei is calculated by using the modified version of the code JULIAN [28], which follows the correct procedure of angular momentum coupling at each stage of de-excitation. The code can be used to study high-energy heavy-ion reactions. The transmission coefficients for light-particle emission are determined from the optical model potential where all the optical model parameters are kept as default. The shift in the coulomb barrier during de-excitation is accounted by calculating the transmission coefficients at an effective energy determined by the shift. The code internally decides the level densities and masses it needs during de-excitation. The Gilbert-Cameron level density is adopted in the calculation. Fission is considered as a decay mode, and the fission barrier can be changed accordingly in the program. The default fission barrier is the Cohen-Plasil-Swiatecki rotating liquid-drop fission barrier. The saddle-point level density is proportional to the a parameter. For compound nucleus reactions, distributions are determined as a function of angle around the recoil axis, and for deep inelastic products, angular distributions are determined as functions of the angle axis perpendicular to the reaction plane. The compound nuclear fusion cross section is determined by using the Bass method [29]. A nonstatistical yrast cascade γ-decay chain has been artificially incorporated to simulate γ multiplicity and energy results.

III. IMPORTANT FEATURES OF THE CODES

(i) TALYS uses an exciton model to calculate PEQ emissions followed by a Hauser-Feshbach formalism for EQ emissions. ALICE91 uses a hybrid model for PEQ and a Weisskopf-Ewing formalism for EQ emissions.

(ii) TALYS relies on DIR emissions treated by coupled channel analysis, DWBA [30], giant resonance [31,32], etc. However, ALICE91 does not consider DIR emissions.

(iii) Direct-like processes (e.g., stripping, pickup, and knockout) play an important role in nuclear reactions involving clusters ($d, t,{}^3$He, and α particles) as projectile and ejectile. TALYS includes these processes in the framework of Kalbach's phenomenological model. ALICE91 does not take into account these processes.

(iv) TALYS considers n, p, d, $t,{}^3$He, and α particles as both projectile and ejectile with single and simultaneous emission of any order in PEQ and EQ emissions. ALICE91 considers light particles up to α particles as projectile but only n, p, d, and α particles are considered as ejectiles. Single and simultaneous emission of two nucleons are taken into account in PEQ emissions, and, for EQ reactions, n, p, d, and α-particle emissions are calculated from successive residuals. PEQ emissions from heavy-ion-induced reactions can also be calculated by using a hybrid model in ALICE91 with necessary modifications.

(v) PACE-II is a Monte Carlo statistical code based on Hauser-Feshbach formalism and the decay channels consider statistical emission of γ rays, n, p, and α particles.

IV. RESULTS AND DISCUSSION

In the present report excitation functions of $^{209-211}$At have been calculated by using the reaction model codes TALYS, ALICE91, and PACE-II produced through various possible target-projectile combinations in the incident energy range starting from threshold to 100 MeV. Table II represents the details of reactions with the reaction threshold values. Production of $^{209-211}$At through ^{209}Bi(α, xn) and ^{209}Bi$(^3\mathrm{He}, xn)$ reactions have been studied by using the codes TALYS and ALICE91 and have been compared with the available experimental cross sections. Other possible production routes of At radionuclides via heavy-ion-induced reactions have been studied by using the codes ALICE91 and PACE-II and have also been compared with the available measured data. It has been seen that all the measured excitation functions of ^{211}At [5,33–35] produced through the ^{209}Bi$(\alpha, 2n)^{211}$At reaction are in good agreement with each other.

It has been seen earlier that α particles may interact with the target nucleons in different ways. Among others, two modes of interaction to the total reaction cross section make a 95% contribution: (i) one in which an α particle dissolves into four constituent nucleons in the nuclear force field ($n_0 = 4$; 4p-0h) [36,37] and (ii) another in which an α particle as a whole interacts with a target nucleon and creates a particle-hole pair, which is the starting point of the PEQ cascade ($n_0 = 6$; 5p-1h). It has also been found that both these initial configurations have proportional contribution to the angular distribution of the ejectiles [38]. ALICE91 has an option to select the initial exciton number n_0 in its input. We have performed separate calculations of excitation functions for both the options $n_0 = 4$ and 6. The resultant excitation functions of $^{209-211}$At have been calculated by taking a 70% contribution from $n_0 = 6$ and a 30% contribution from $n_0 = 4$ according to the observation of Gadioli and Gadioli-Erba [39].

Figure 1 shows a comparison between the formation cross section of $^{209-211}$At produced from ^{209}Bi via $(\alpha, 2n)$, $(\alpha, 3n)$, and $(\alpha, 4n)$ reaction channels calculated using TALYS and ALICE91. In the TALYS calculation, an optical model has been used to calculate the inverse reaction cross section with the default level density option, which is a combination of the constant-temperature model of Gilbert and Cameron [25] and the Fermi gas model. In the ALICE91 calculation we have used an optical model with the Fermi gas level density option. All three isotopes of At are well separated from each other and the

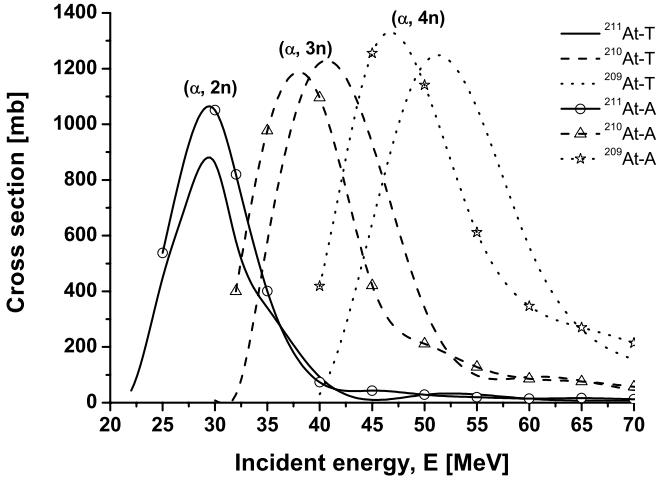

FIG. 1. Comparison between the calculated excitation functions of $^{209-211}$At radionuclides from the reaction ^{209}Bi$(\alpha, xn)^{209-211}$At using the codes TALYS (lines) and ALICE91 (lines with symbols).

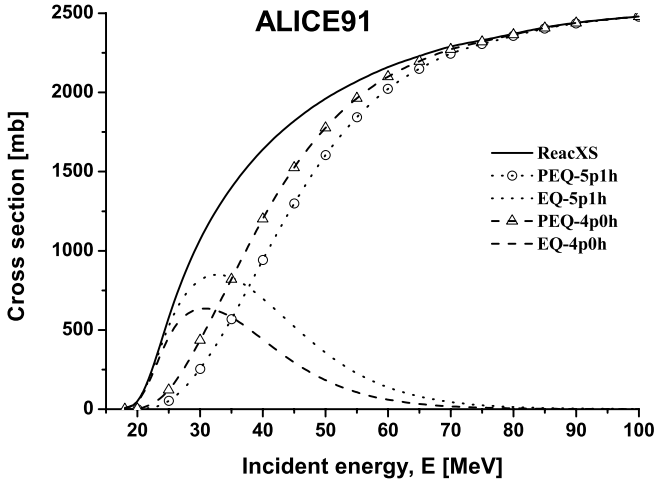

FIG. 3. Contribution of PEQ and EQ reactions to the total cross section as obtained from ALICE91 for two initial exciton numbers ($n_0 = 4$; 4p-0h and $n_0 = 6$; 5p-1h) for α-induced reaction on ^{209}Bi.

maximum productions of ^{211}At and ^{210}At have also been seen at incident energies of 30 and 40 MeV, respectively, in both results. However, ALICE91 produces 20% more ^{211}At and 10% less ^{210}At than TALYS. The maximum production of ^{209}At is at 45 MeV in ALICE91 and at 50 MeV in TALYS.

To investigate the results obtained from the two model codes, we have studied the contributions from the reaction mechanisms involved in α-induced reactions on a ^{209}Bi target. Contributions from PEQ, EQ and DIR reactions to the total reaction cross section have been shown against incident projectile energy as obtained from TALYS and ALICE91 separately in Figs. 2 and 3. Figure 2 shows that, up to 100 MeV incident energy, there is almost no contribution from the direct reaction. One can see no PEQ reaction contribution at low incident energies; however, the PEQ component increases with increasing incident energy. The most dominant component is the EQ reaction in the range considered for the present work. It follows a similar increasing trend up to 50 MeV with

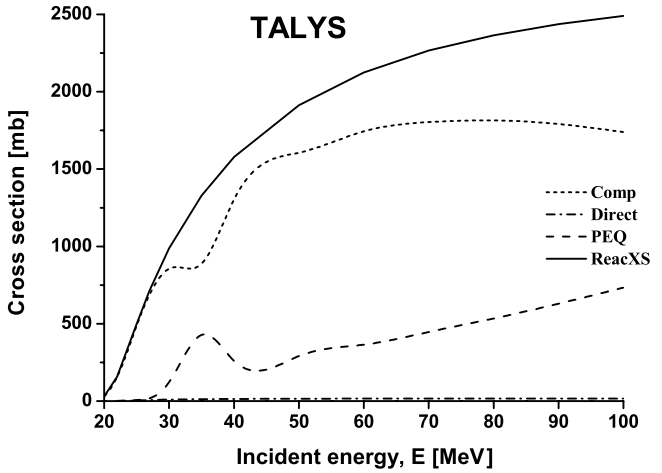

FIG. 2. Contribution of different reaction mechanisms (DIR, PEQ, and EQ) to the total reaction cross section (ReacXS) as obtained from TALYS for $\alpha + ^{209}$Bi.

the total reaction cross section, which shows an increasing trend through the entire energy range considered. The rate of increment of the EQ cross section is slow at the higher incident energies as the PEQ component is increasing with increasing incident energy. For ALICE91 in Fig. 3, we see that the EQ contribution is significant only at low energies for both initial configurations (4p-0h and 5p-1h) of α-induced reactions. The PEQ component is increasing rapidly with increasing incident energy for both initial exciton numbers. The total cross section also shows an increasing trend throughout the range. The PEQ contribution from the 5p-1h configuration is less than that of the 4p-0h configuration up to an energy of 60 MeV. This is because, for the 5p-1h configuration, the PEQ emission starts in the hybrid model calculation from $n_0 = 6$, which is one stage later than $n_0 = 4$. As a result, the PEQ contribution is larger for $n_0 = 4$ than for $n_0 = 6$. It is observed from the plot that the total PEQ cross section does not increase above 60 MeV for either case. This is because the code ALICE91 has a cutoff value ($= n_0 + 18$) of n_0 if it exceeds this value. The case of the EQ reaction is just the reverse between $n_0 = 4$ and $n_0 = 6$. This is because after sufficient PEQ emission from the 4p-0h configuration the total available excitation becomes low, which in turn reduces the EQ emission.

Though the favored production route of $^{209-211}$At is from α-induced reactions on the Bi target, it is also possible to produce $^{209-211}$At by using light- and heavy-ion-induced reactions. In this report, we have found possible production routes of $^{209-211}$At from ^{6,7}Li- and ^{9}Be-induced reactions on ^{nat}Pb and ^{nat}Tl targets. Figures 4–6 represent the comparative study of the formation cross section of $^{209-211}$At produced through (^{7}Li, xn), (^{6}Li, xn), and (^{9}Be, xn) reactions on ^{nat}Pb and ^{nat}Tl targets using the codes ALICE91 and PACE-II.

The four naturally occurring isotopes of Pb are ^{208}Pb (52.4%), ^{207}Pb (22.1%), ^{206}Pb (24.1%), and ^{204}Pb (1.4%). Thallium has two naturally occurring isotopes, ^{205}Tl (70.5%) and ^{203}Tl (29.5%). The formation cross sections have been calculated separately from each isotope of Pb by using ^{7}Li and ^{6}Li projectiles and that from ^{9}Be-induced reactions on

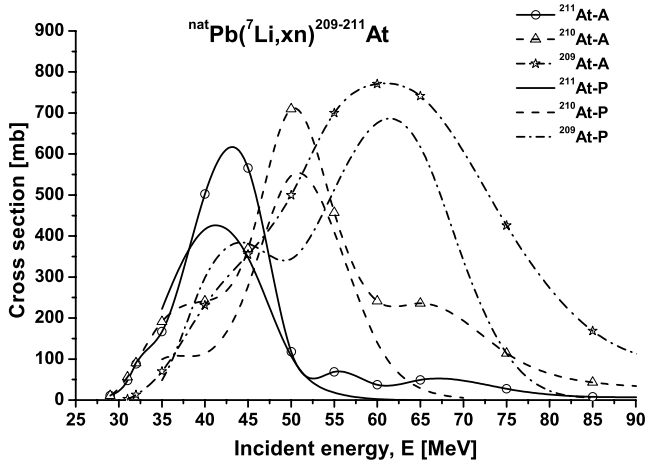

FIG. 4. Comparison between the formation cross sections of $^{209-211}$At from ^{7}Li-induced reactions on a ^{nat}Pb target using ALICE91 and PACE-II.

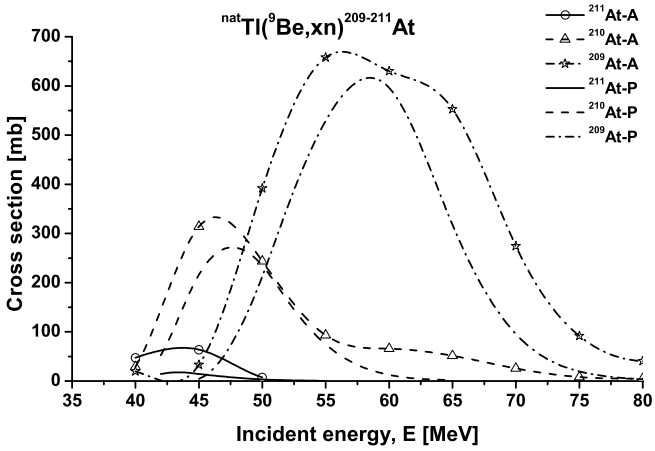

FIG. 6. Comparison between the formation cross sections of $^{209-211}$At from ^{9}Be-induced reactions on a ^{nat}Tl target using ALICE91 and PACE-II.

Tl isotopes. The total formation cross section is calculated by taking the weighted average of all the naturally occurring isotopes. The same procedure has been followed for the results obtained from both the codes ALICE91 and PACE-II.

The total formation cross section obtained from ALICE91 is the sum of PEQ and EQ cross sections. For the PEQ calculation of heavy-ion-induced reactions in the framework of the hybrid model, we have considered the initial exciton number as the total number of nucleons in the projectile. The EQ cross section is calculated using the Weisskopf-Ewing formalism. The formation cross sections obtained from PACE-II is only from the evaporation calculation following the Hauser-Feshbach formalism.

In Figs. 4 and 5, production cross sections of $^{209-211}$At obtained from ALICE91 are larger than those obtained from PACE-II but the maximum production cross section is obtained at a particular incident energy for both model calculations. Production of ^{211}At is not significant in ^{6}Li-induced reactions on a ^{nat}Pb target. However, ^{209,210}At will be produced in significant amounts in both ^{7}Li- and ^{6}Li-induced reactions on a natural Pb target. Figure 6 shows the production cross section of $^{209-211}$At radionuclides from ^{9}Be-induced reactions on a ^{nat}Tl target. Almost no production of ^{211}At is seen in this case with sufficiently good production of two other radionuclides. In all three cases (Figs. 4–6), the ALICE91 prediction is larger than that of PACE-II. This may be due to the added contribution from PEQ reactions in ALICE91.

In Figs. 7 and 8, we have compared the measured production cross sections of ^{211}At [10] and ^{210}At [5,10,40,41] produced from α-induced reactions on a ^{209}Bi target through $(\alpha, 2n)$ and $(\alpha, 3n)$ channels reported by several authors with the theoretical predictions obtained from TALYS, ALICE91, and PACE-II. Figure 7 shows that TALYS perfectly matches with the measured data of ^{211}At [10] in the range shown. ALICE91 also matches with the measured data except at low energies. PACE-II reproduces the data up to 32 MeV. It underpredicts the data, showing a abrupt fall in the cross section above 32 MeV. This comparison reveals that the PEQ reaction mechanism plays an important role in reproducing the measured data. We have seen in Fig. 2 that in the energy range up to 100 MeV,

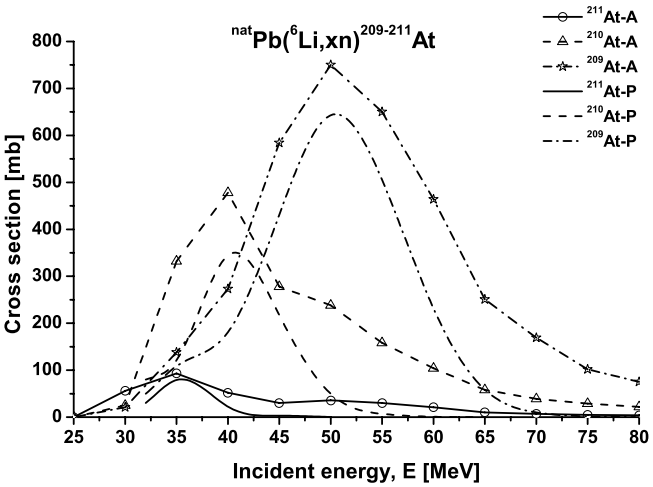

FIG. 5. Comparison between the formation cross sections of $^{209-211}$At from ^{6}Li-induced reactions on a ^{nat}Pb target using ALICE91 and PACE-II.

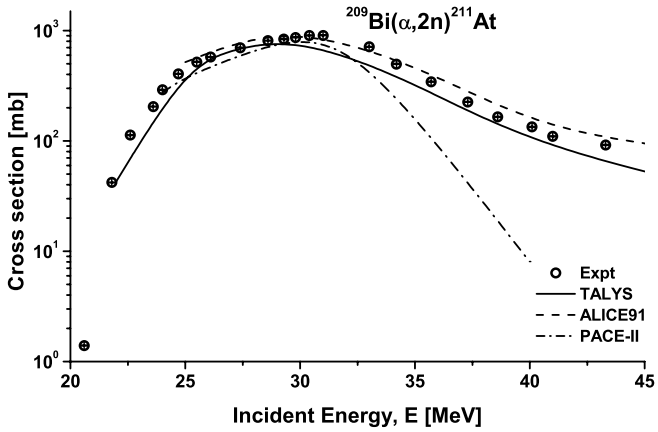

FIG. 7. Comparison of measured formation cross section [10] of ^{211}At from α-induced reactions on ^{209}Bi with the TALYS, ALICE91, and PACE-II predictions.

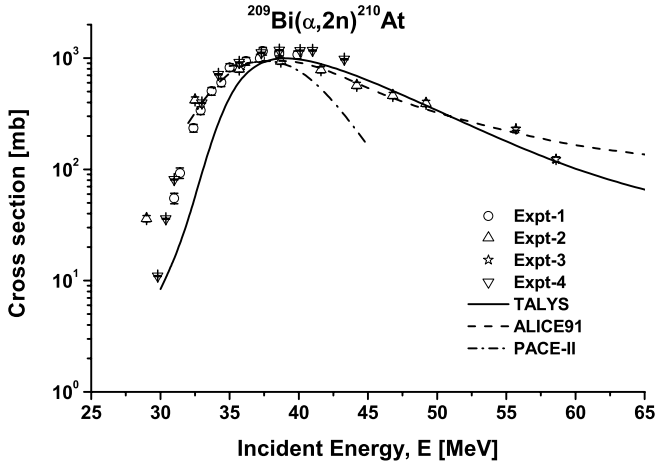

FIG. 8. Same as Fig. 7 but for ^{210}At [5,10,40,41].

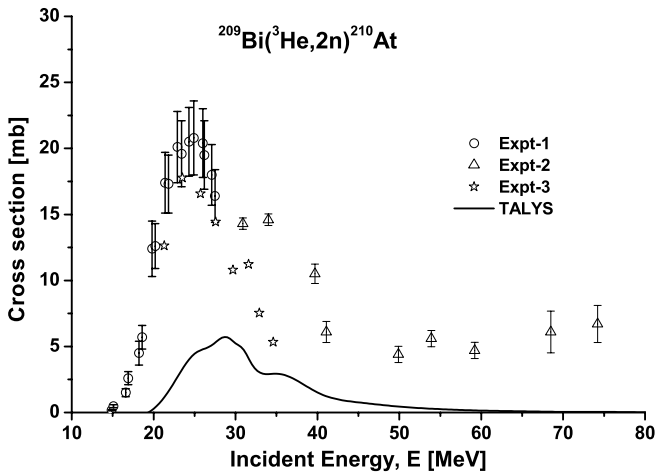

FIG. 9. Comparison of measured formation cross section of ^{210}At from ^{3}He-induced reactions [42–44] on ^{209}Bi using TALYS.

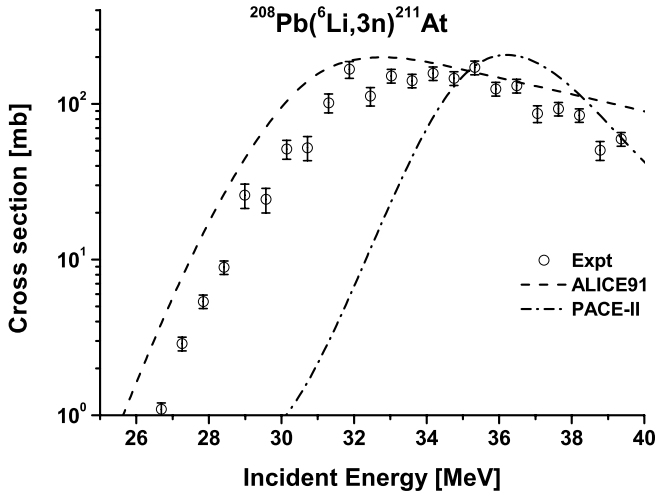

FIG. 10. Comparison of measured formation cross section of ^{211}At from ^{6}Li-induced reactions [45] on ^{208}Pb with the ALICE91 and PACE-II calculations.

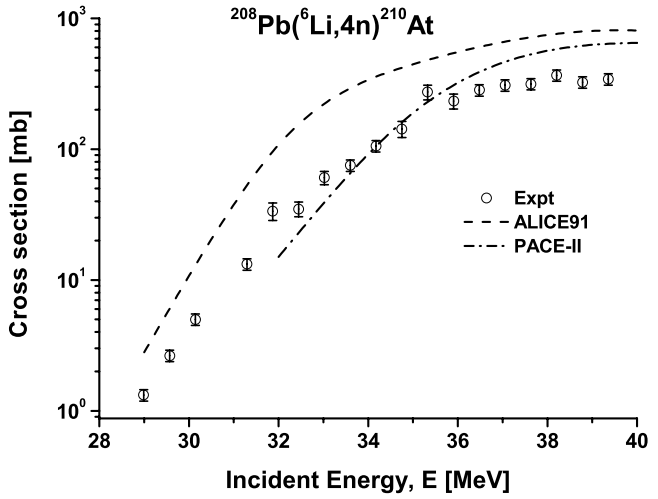

FIG. 11. Same as Fig. 10 but for ^{210}At [45].

the DIR reaction has absolutely no role. As TALYS and ALICE91 account for the PEQ reactions along with EQ reaction, they produce the measured data satisfactorily. Figure 8 shows that TALYS also evaluates the measured formation cross section of ^{210}At. ALICE91 produces the data well but not below 32 MeV. PACE-II shows the same nature as the production of ^{211}At.

Figure 9 compares the measured excitation function of ^{210}At from ^{3}He-induced reactions [42–44] on a ^{209}Bi target with the TALYS predicted value. The trend of the measured data is well reproduced by TALYS, but its absolute value underpredicts the measured data by a factor of 5. ALICE91 fails to produce the data. Figures 10 and 11 present comparisons between measured data of ^{211}At and ^{210}At produced from ^{208}Pb(^{6}Li, $3n$)^{211}At [45] and ^{208}Pb(^{6}Li, $4n$)^{210}At [45] reactions with the theoretical values from ALICE91 and PACE-II. From Fig, 10, it is observed that formation cross section of ^{211}At is well reproduced by the calculated values of ALICE91 within the uncertainty range. However, PACE-II only reproduces the higher energy side of the spectrum. For the formation cross section of ^{210}At in Fig. 11, ALICE91 and PACE-II both

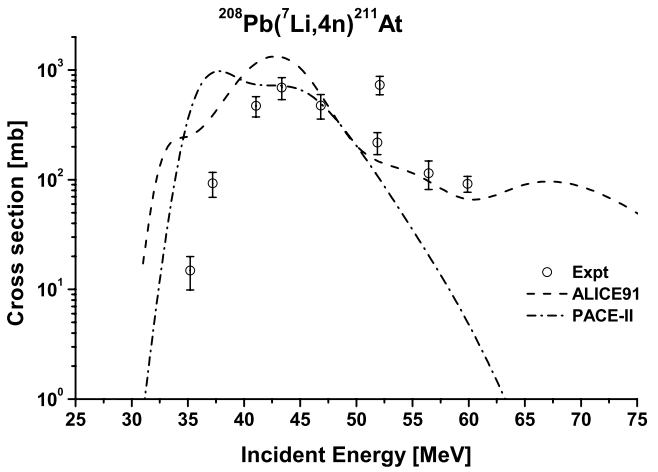

FIG. 12. Comparison of measured formation cross section of ^{211}At from ^{7}Li-induced reactions on ^{208}Pb [46] with the ALICE91 and PACE-II calculations.

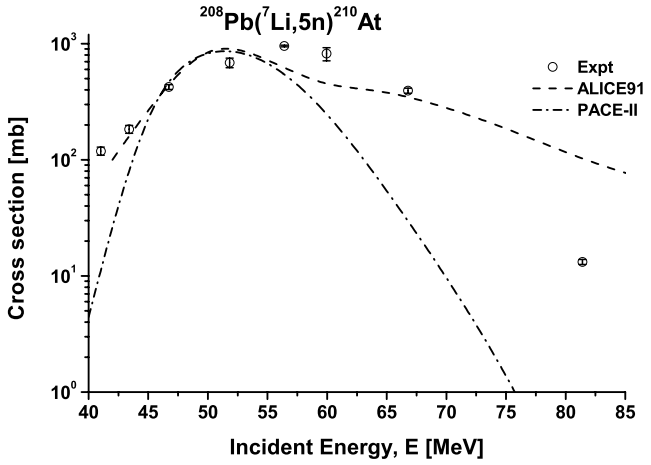

FIG. 13. Same as Fig. 12 but for ^{210}At [46].

reproduce the trend of the measured data. The absolute values of the cross section obtained from PACE-II produce the measured data, whereas ALICE91 slightly overpredicts the data.

In a similar fashion, we have compared production of ^{211}At [46] and ^{210}At [46] from ^{7}Li-induced reactions on a ^{208}Pb target. The trend of measured cross section of ^{211}At in Fig. 12 is well reproduced by ALICE91 but the absolute value of the cross sections overpredicts the measured data below 45 MeV. PACE-II produces neither the trend nor the absolute values of cross section except for the particular energy of 45 MeV. In Fig. 13, we see that ALICE91 explains the measured data well but PACE-II underpredicts the data mostly.

V. CONCLUSIONS

The study of heavy-ion-induced production of $^{209-211}$At radionuclides shows that the PEQ reaction mechanism plays an important role in the energy range studied and that performance of the ALICE91 code is better in most cases. PACE-II does not consider the PEQ reaction in its calculation and therefore mostly underpredicts the measured data at the high-energy side where the PEQ reaction contributes. The excitation functions of At radionuclides from α-induced reactions calculated by the codes TALYS and ALICE91 are comparable and both agree with the experimental data at higher energies. However, the cross sections at low energies are well reproduced by TALYS. Heavy-ion-induced production cross sections of $^{209-211}$At obtained from ALICE91 are mostly in good agreement with the measured data, whereas PACE-II calculations underpredict them. This may be due to the significant contribution from PEQ reactions, which is accounted in ALICE91. This study on the contribution of various reaction mechanisms to the total cross section agrees with the fact that the direct reaction plays no role in the production of At radionuclides from either light- or heavy-ion-induced reactions.

ACKNOWLEDGMENTS

This work has been carried out as part of the Saha Institute of Nuclear Physics-Department of Atomic Energy, XI five-year plan project "Trace Analysis: Detection, Dynamics and Speciation (TADDS)."

[1] K. Roy and S. Lahiri, Appl. Radiat. Isot. **66**, 571 (2008).
[2] K. Roy, S. Basu, A. Ramaswami, D. Nayak, and S. Lahiri, Appl. Radiat. Isot. **60**, 793 (2004).
[3] D. Nayak and S. Lahiri, Radiochim. Acta **91**, 159 (2003).
[4] E. Browne and R. B. Firestone, *Table of Radioactive Isotopes* (Wiley, New York, 1986).
[5] A. Hermanne, F. Trknyi, S. Takcs, Z. Szücs, Yu. N. Shubin, and A. I. Dityuk, Appl. Radiat. Isot. **63**, 1 (2005).
[6] O. Lebeda, R. Jiran, J. Rli, and J. Tursa, Appl. Radiat. Isot. **63**, 49 (2005).
[7] G. Henriksen, S. Messelt, E. Olsen, and R. H. Larsen, Appl. Radiat. Isot. **54**, 839 (2001).
[8] M. K. Schultz, M. Hammond, J. T. Cessna, P. Plascjak, B. Norman, L. Szajek, K. Garmestani, B. E. Zimmerman, and M. Unterweger, Appl. Radiat. Isot. **64**, 1365 (2006).
[9] F. Groppi, M. L. Bonardi, C. Birattari, E. Menapace, K. Abbas, U. Holzwarth, A. Alfarano, S. Morzenti, C. Zona, and Z. B. Alfassi, Appl. Radiat. Isot. **63**, 621 (2005).
[10] W. J. Ramler, J. Wing, D. J. Henderson, and J. R. Hvizenga, Phys. Rev. **114**, 154 (1959).
[11] R. H. Larsen, B. W. Wieland, and M. R. Zalutsky, Appl. Radiat. Isot. **47**, 135 (1996).
[12] A. J. Koning, S. Hilarie, and M. C. Duijvestijn, AIP Conf. Proc. **769**, 1154 (2005).
[13] M. Blann, Lawrence Livermore National Laboratory Report No. UCID 19614 (1982); M. Blann, International Centre for Theoretical Physics Workshop on Applied Nuclear Theory and Nuclear Model Calculations for Nuclear Technology Applications, Trieste, Italy, SMR/284-1, 1988.
[14] M. Blann and H. K. Vonach, Phys. Rev. C **28**, 1475 (1983).
[15] A. Gavron, Phys Rev. C **21**, 230 (1980).
[16] W. Hauser and H. Feshbach, Phys. Rev. **87**, 366 (1952).
[17] V. F. Weisskopf and D. H. Ewing, Phys. Rev. **57**, 472 (1940).
[18] M. Blann, Phys. Rev. Lett. **27**, 337 (1971); **27**, 700(E) (1971); **27**, 1550(E) (1971).
[19] M. Blann, Nucl. Phys. **A213**, 570 (1973).
[20] M. Blann, Phys. Rev. Lett. **28**, 757 (1972).
[21] J. J. Griffin, Phys. Rev. Lett. **17**, 478 (1966).
[22] G. D. Harp, J. M. Miller, and B. J. Berne, Phys. Rev. **165**, 1166 (1968).
[23] G. D. Harp and J. M. Miller, Phys. Rev. C **3**, 1847 (1971).
[24] C. Kalbach, Phys. Rev. C **71**, 034606 (2005).
[25] A. Gilbert and A. G. W. Cameron, Can. J. Phys. **43**, 1446 (1965).
[26] P. A. Moldauer, Phys. Rev. C **14**, 764 (1976).
[27] P. A. Moldauer, Nucl. Phys. **A344**, 185 (1980).
[28] M. Hillman and Y. Eyal (unpublished).
[29] R. Bass, Phys. Rev. Lett. **39**, 265 (1977).
[30] G. R. Satchler, *Direct Nuclear Reactions* (Oxford University Press, New York, 1983).

[31] A. van der Woude, *Electric and Magnetic Giant Resonances in Nuclei* (World Scientific, Singapore, 1991), pp. 99–232.
[32] C. Kalbach, Phys. Rev. C **62**, 044608 (2000).
[33] G. Deconninck and M. Longree, Ann. Soc. Sci. Bruxelles **88**, 341 (1974).
[34] R. M. Lambrecht and S. Mirzadeh, Appl. Radiat. Isot. **36**, 443 (1985).
[35] W. J. Ramler, J. Wing, D. J. Henderson, and J. R. Huizenga, Phys. Rev. **114**, 154 (1959).
[36] M. Blann, Annu. Rev. Nucl. Sci. **25**, 123 (1975).
[37] E. Gadioli, Nukleonika **21**, 385 (1976).
[38] M. Maiti, S. N. Roy, M. Nandy, and P. K. Sarkar, Phys. Rev. C **71**, 034601 (2005).
[39] E. Gadioli and E. Gadioli-Erba, Z. Phys. A **299**, 1 (1981).
[40] N. L. Singh, S. Mukherjee, and D. R. S. Somayajulu, Nuovo Cimento A **107**, 1635 (1994).
[41] S. S. Rattan, N. Chakravarty, A. Ramaswami, and R. J. Singh, Radiochim. Acta **57**, 7 (1992).
[42] Z. Szucs, F. Szelecsenyi, J. Bergmann, S. J. Heselius, and O. Solin, Radiochim. Acta **65**, 87 (1994).
[43] O. N. Vysotsky, A. V. Gonchar, G. N. Kozeratskaya, S. N. Kondratiev, V. D. Sklyarenko, and V. V. Tokarevsky, Izv. Ross. Akad. Nauk, Ser. Fiz. **56**, 102 (1992).
[44] Y. Nagame, Y. Nakamura, M. Takahashi, K. Sueki, and H. Nakahara, Nucl. Phys. **A486**, 77 (1988).
[45] Y. W. Wu, Z. H. Liu, C. J. Lin, H. Q. Zhang, M. Ruan, F. Yang, Z. C. Li, M. Trotta, and K. Hagino, Phys. Rev. C **68**, 044605 (2003).
[46] A. A. Hassan, S. M. Luk'yanov, R. Kalpakchieva, Yu. E. Penionzhkevich, R. A. Astabatyan, I. Vintsour, Z. Dlougy, A. A. Kul'ko, Ya. Mrazek, S. P. Lobastov, E. R. Markaryan, V. A. Maslov, N. K. Ckobelev, and Yu. G. Sobolev, Izv. Ross. Akad. Nauk, Ser. Fiz. **70**, 1558 (2006).